

Supporting Information for

Stepwise modulation of the electron-donating strength of ancillary ligands: understanding the AIE mechanism of cationic iridium(III) complexes

Yong Wu,^a Hai-Zhu Sun,^a Hong-Tao Cao,^a Hai-Bin Li,^a Guo-Gang Shan,^{*a} Yu-Ai Duan,^a Yun Geng,^a Zhong-Min Su^{*a} and Yi Liao^{*b}

^aInstitute of Functional Material Chemistry, Faculty of Chemistry, Northeast Normal University, Changchun 130024, People's Republic of China.

Fax: +86-431-85684009, Tel.: +86-431-85099108.

E-mail: shangg187@nenu.edu.cn, zmsu@nenu.edu.cn

^bDepartment of Chemistry, Capital Normal University, Beijing, People's Republic of China.

E-mail: liaoy271@nenu.edu.cn

1. Experimental general information

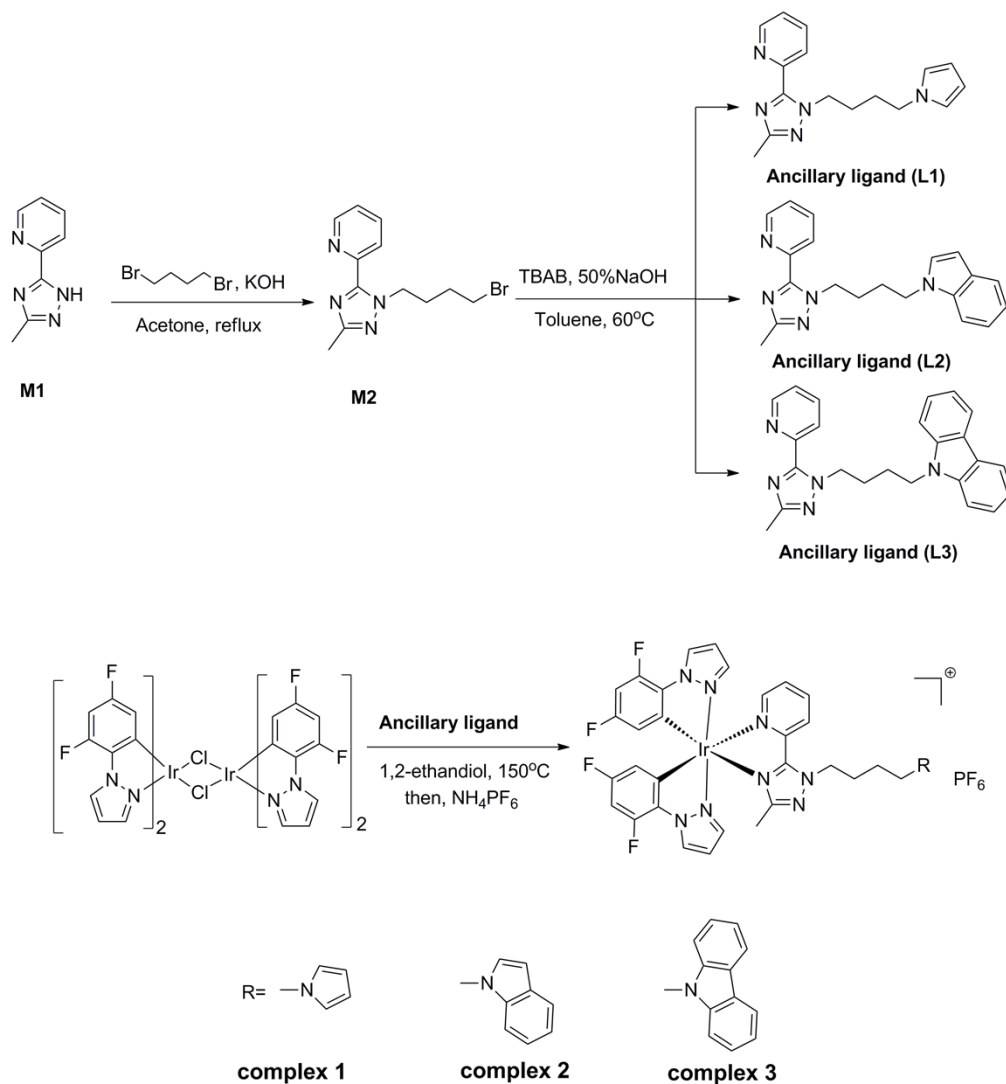
All reagents and solvents employed were commercially available and used as received without further purification. The solvents for syntheses were freshly distilled over appropriate drying reagents. All experiments were performed under a nitrogen atmosphere by using standard Schlenk techniques. ^1H NMR spectra were measured on Bruker Avance 500 MHz with tetramethylsilane as the internal standard. The molecular weights of ligands and complexes were tested by using electrospray-ionization mass spectroscopy and matrix-assisted laser desorption-ionization time-of-flight (MALDI-TOF) mass spectrometry, respectively. The emission spectra were recorded using the F-4500 FL spectrophotometer. The excited-state lifetime were measured on a transient spectrofluorimeter (Edinburgh FLS920) with time-correlated single-photon counting technique. The photoluminescence quantum yields (PLQYs) of the neat film were measured in an integrating sphere. The doped-PMMA films were prepared by dissolving 5.0 mg of the studied complexes and corresponding concentrations of PMMA in 2 mL of CH_2Cl_2 followed by coating 0.5 mL resulting solution onto the surface of a quartz cell or other substrate. After slow evaporation of the solvent, the film was further dried at 60 °C in a vacuum over for 2 h before it was used for PL measurement.

2. Synthesis and characterization of corresponding ancillary ligand (L1-L3) and cationic Ir(III) complexes 1-3

2.1 Synthesis of 2-(1-(4-bromobutyl)-3-methyl-1*H*-1,2,4-triazol-5-yl)pyridine (M2)

A mixture of the precursor 2-(3-methyl-1*H*-1,2,4-triazol-5-yl)pyridine (M1) (0.8 g, 5.0 mmol) prepared according to previous report² was dissolved in acetone (30 mL), and the equivalent KOH was added and the mixture was stirred for 0.5 h. Then, 1,4-dibromobutane (1.18 g, 5.5 mmol) in 5 mL acetone was added into the reaction system and the mixture was heated to reflux for overnight. After cooling to room temperature, the mixture was quenched by water and then extracted by dichloromethane. The organic layer was dried with Na_2SO_4 and the solvent was removed. The obtained residues was purified by column chromatography on silica

gel with ethyl acetate/petroleum ether (1:3) as the eluent to yield the white solid (58%). ^1H NMR (500 MHz, CDCl_3 , ppm): δ 8.66–8.67 (m, 1H), 8.19 (d, $J = 8$ Hz, 1H), 7.80–7.84 (m, 1H), 7.33–7.35 (m, 1H), 4.81 (t, $J = 7.0$ Hz, 2H), 3.46 (t, $J = 7.0$ Hz, 2H), 2.44 (s, 3H), 2.05–2.11 (m, 2H), 1.89–1.95 (m, 2H).



Scheme S1 Synthetic routes of ancillary ligand and the cationic Ir(III) complexes studied in this work.

2.2 Synthesis of ancillary ligand (L1)

A mixture of **M2** (0.99 g 3.36 mmol), pyrrole (0.30 g, 4.5 mmol), 50%NaOH (10mL) and tetrabutyl ammonium bromide (TBAB, 0.8 g) in 25 mL toluene was heated at 60°C for 6 h under argon. After cooling to room temperature, the mixture was extracted with CH_2Cl_2 . After washing with water, drying over anhydrous Na_2SO_4 , and evaporating the solvents, we purified the residue by column

chromatography on silica gel using the ethyl acetate/petroleum ether (1:6) as eluent, yielding **L1**. Yield: 57%. ¹H NMR (500 MHz, CDCl₃, ppm): δ 8.63–8.64 (m, 1H), 8.18 (d, *J* = 8.0 Hz, 1H), 7.80–7.83 (m, 1H), 7.32–7.34 (m, 1H), 6.61 (d, *J* = 2.0 Hz, 2H), 6.11 (d, *J* = 2.0 Hz, 1H), 4.79 (t, *J* = 7.0 Hz, 2H), 3.91 (t, *J* = 7.0 Hz, 2H), 2.44 (s, 3H), 1.90–1.94 (m, 2H), 1.80–1.84 (m, 2H).

2.2 Synthesis of ancillary ligand (L2)

The synthesis of ancillary ligand **L2** was similar to that of **L1** except that the pyrrole was replaced with indole. ¹H NMR (500 MHz, CDCl₃, ppm): 8.57 (d, *J* = 4.5 Hz, 1H), 8.17 (d, *J* = 8.0 Hz, 1H), 7.78–7.81 (m, 1H), 7.62 (d, *J* = 8.0 Hz, 1H), 7.29–7.32 (m, 2H), 7.19 (t, *J* = 7.5 Hz, 1H), 7.10 (t, *J* = 7.5 Hz, 1H), 7.05 (d, *J* = 3.0 Hz, 1H), 6.46 (d, *J* = 3.0 Hz, 1H), 4.79 (t, *J* = 7.0 Hz, 2H), 4.16 (t, *J* = 7.0 Hz, 2H), 2.44 (s, 3H), 1.87–1.96 (m, 4H).

2.3 Synthesis of ancillary ligand (L3)

The synthesis of ancillary ligand **L3** was similar to that of **L1** except that the pyrrole was replaced with carbazole. The obtained ¹H NMR data is same as our previously one. ¹H NMR (500 MHz, CDCl₃, ppm): δ 8.52 (d, *J* = 4.0 Hz, 1H), 8.14 (d, *J* = 8.0 Hz, 1H), 8.07 (d, *J* = 7.5 Hz, 2H), 7.34–7.77 (m, 1H), 7.40–7.43 (m, 2H), 7.34–7.36 (m, 2H), 7.25–7.26 (m, 1H), 7.18–7.24 (m, 2H), 4.77 (t, *J* = 7.0 Hz, 2H), 4.31 (t, *J* = 7.0 Hz, 2H), 2.43 (s, 3H), 1.97–2.01 (m, 2H), 1.89–1.92 (m, 2H).

2.4 Synthesis of the chloro-bridged dimer [Ir(dfppz)₂Cl]₂

The organometallated dimer [Ir(dfppz)₂Cl]₂ was synthesized from reaction of IrCl₃·3H₂O (0.81 g, 2.32 mmol) with 1-(2,4-difluorophenyl)-1*H*-pyrazole (dfppz, 0.92 g, 5.10 mmol) in 2-ethoxyethanol and water mixture (V:V = 3:1, 40 mL) for 24 h. The mixture was treated with water (30 mL) to induce precipitation of the yellow solid. The product was filtered out and washed with diethyl ether followed by ethanol and dried (yield: 70%).

2.5 Synthesis and characterization of [Ir(dfppz)₂(L1)](PF₆) (1)

A solution of ligand **L1** (0.59 g, 2.1 mmol) and the dichloro-bridged diiridium

complex $[\text{Ir}(\text{dfppz})\text{Cl}]_2$ (1.2 g, 1.0 mmol) in 1,2-ethandiol (30 ml) was heated at 150 °C for 12 h in the dark. After cooling to room temperature, the aqueous solution of NH_4PF_6 (1.8 g in 100 mL of deionized water) was slowly added into the reaction mixture under stirring. The obtained yellow suspension was filtrated, and washed with water and methanol. The crude product was purified by silica gel column chromatography using the ethyl acetate/petroleum ether (1:6) to reduce the excessive ancillary ligand **L1**, followed by the dichloromethane/ethyl acetate (3:2). The product was then recrystallized from dichloromethane and petroleum ether mixture, yielding a white powder (71%). ^1H NMR (500 MHz, d_6 -DMSO, ppm): δ 8.63–8.65 (m, 2H), 8.49 (d, $J = 8.0$ Hz, 1H), 8.34 (t, $J = 8.0$ Hz, 1H), 8.04 (d, $J = 5.5$ Hz, 1H), 7.72 (t, $J = 6.5$ Hz, 1H), 7.26 (d, $J = 2.0$ Hz, 1H), 7.04–7.16 (m, 2H), 6.83 (t, $J = 2.0$ Hz, 1H), 6.80 (t, $J = 2.0$ Hz, 1H), 6.72 (s, 2H), 5.95 (t, $J = 2.0$ Hz, 2H), 5.58–5.59 (m, 2H), 4.65–4.73 (m, 2H), 3.92–3.94 (m, 2H), 1.82–1.88 (m, 4H), 1.71 (s, 3H). ^{19}F NMR (470 MHz, d_6 -DMSO, ppm): –66.59 (d, $J = 711.1$ Hz, 6F), –109.63 (q, 1F), –110.16 (q, 1F), –119.93 (q, 1F), –120.13 (q, 1F). MS (MALDI-TOF): m/z 832.20 (M–PF₆).

2.6 Synthesis and characterization of $[\text{Ir}(\text{dfppz})_2(\text{L2})](\text{PF}_6)$ (**2**)

The synthesis of complex **2** was similar to that of complex **1** except that the ancillary ligand **L1** was replaced with **L2**. The crude product was also purified by silica gel column chromatography using the same eluent to yield complex **2** (68%). ^1H NMR (500 MHz, d_6 -DMSO, ppm): δ 8.62–8.65 (m, 2H), 8.49 (d, $J = 8.5$ Hz, 1H), 8.30 (t, $J = 8.0$ Hz, 1H), 8.03 (d, $J = 5.5$ Hz, 1H), 7.72 (t, $J = 7.0$ Hz, 1H), 7.63 (d, $J = 2.0$ Hz, 1H), 7.53 (d, $J = 7.5$ Hz, 1H), 7.47 (d, $J = 8.0$ Hz, 1H), 7.36 (d, $J = 3.0$ Hz, 1H), 7.24 (d, $J = 2.0$ Hz, 1H), 7.05–7.14 (m, 3H), 7.02 (t, $J = 7.0$ Hz, 1H), 6.82 (t, $J = 2.5$ Hz, 1H), 6.78 (t, $J = 2.5$ Hz, 1H), 6.42 (d, $J = 3.5$ Hz, 1H), 5.59 (d, $J = 7.5$ Hz, 2H), 4.68–4.75 (m, 2H), 4.23–4.25 (m, 2H), 1.90–1.94 (m, 4H), 1.69 (s, 3H). ^{19}F NMR (470 MHz, d_6 -DMSO, ppm): –66.58 (d, $J = 711.1$ Hz, 6F), –109.62 (q, 1F), –110.15 (q, 1F), –119.91 (q, 1F), –120.11 (q, 1F). MS (MALDI-TOF): m/z 882.23 (M–PF₆).

2.7 Synthesis and characterization of $[\text{Ir}(\text{dfppz})_2(\text{L3})](\text{PF}_6)$ (**3**)

The synthesis of complex **3** was similar to that of complex **1** except that the ancillary ligand **L1** was replaced with **L3**. The obtained ^1H NMR data is same as our previously one. ^1H NMR (500 MHz, d_6 -DMSO, ppm): δ 8.64 (d, $J = 8$ Hz, 1H), 8.60 (d, $J = 3$ Hz, 1H), 8.51 (d, $J = 8$ Hz, 1H), 8.24–8.28 (m, 1H), 8.16 (d, $J = 8$ Hz, 2H), 8.02 (d, $J = 4.5$ Hz, 1H), 7.69–7.72 (m, 1H), 7.59–7.62 (m, 3H), 7.42–7.45 (m, 2H), 7.04–7.21 (m, 5H), 6.79 (t, $J = 2.5$ Hz, 1H), 6.73 (t, $J = 2.5$ Hz, 1H), 5.58 (d, $J = 8$ Hz, 2H), 4.69–4.80 (m, 2H), 4.42–4.47 (m, 2H), 2.01–2.02 (m, 2H), 1.89–1.90 (m, 2H), 1.67 (s, 3H). ^{19}F NMR (470 MHz, d_6 -DMSO, ppm): -66.60 (d, $J = 711.1$ Hz, 6F), -109.62 (q, 1F), -110.13 (q, 1F), -119.89 (q, 1F), -120.10 (q, 1F). MS (MALDI-TOF): m/z 932.22 (M-PF6).

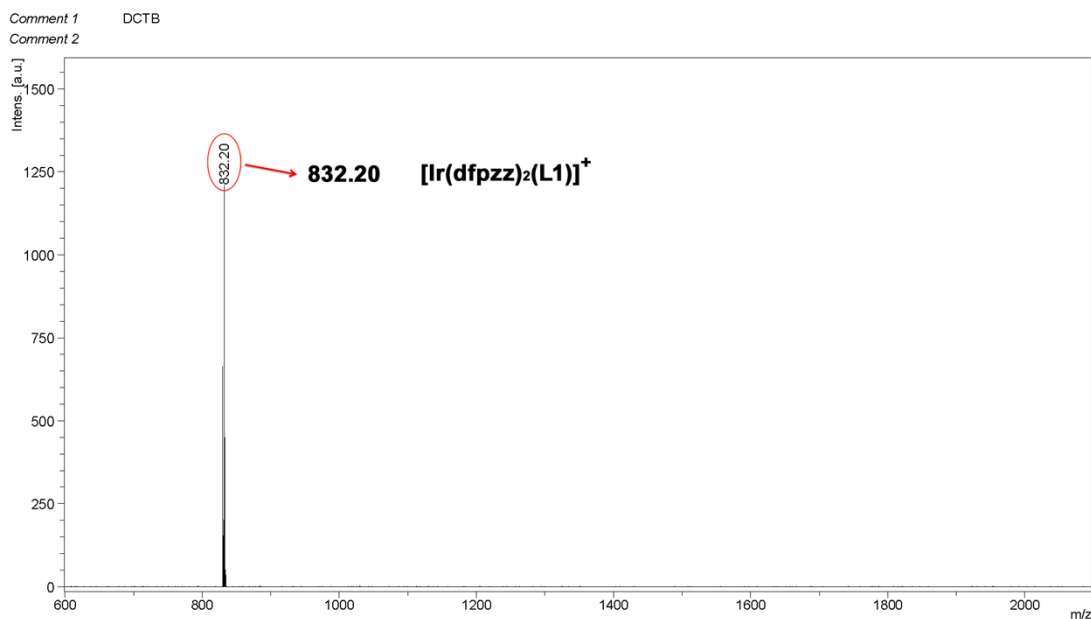


Fig. S1 Copy of the MALDI-TOF MS spectrum for complex **1**.

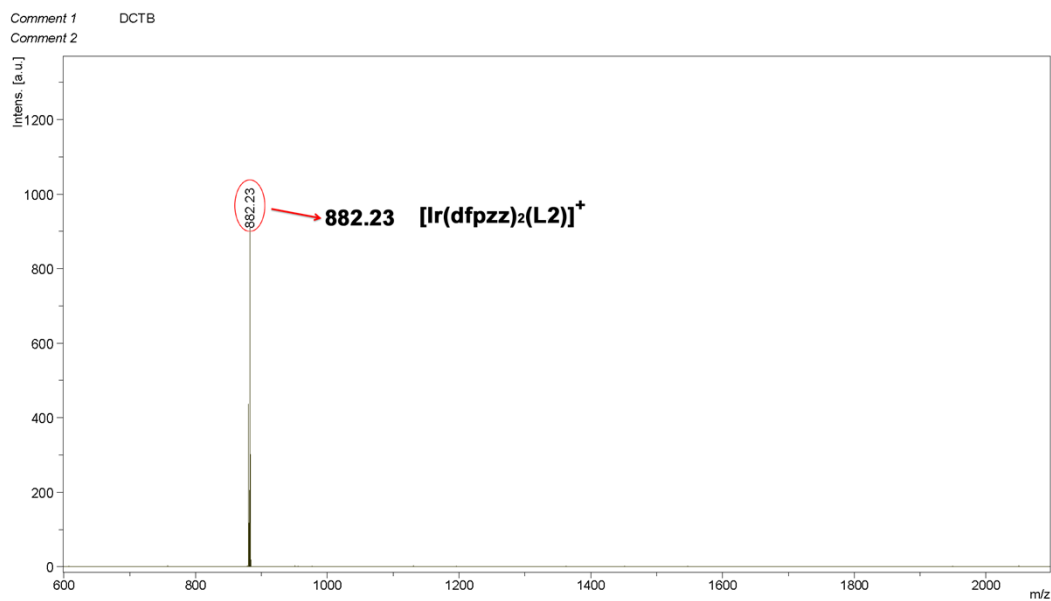


Fig. S2 Copy of the MALDI-TOF MS spectrum for complex **2**.

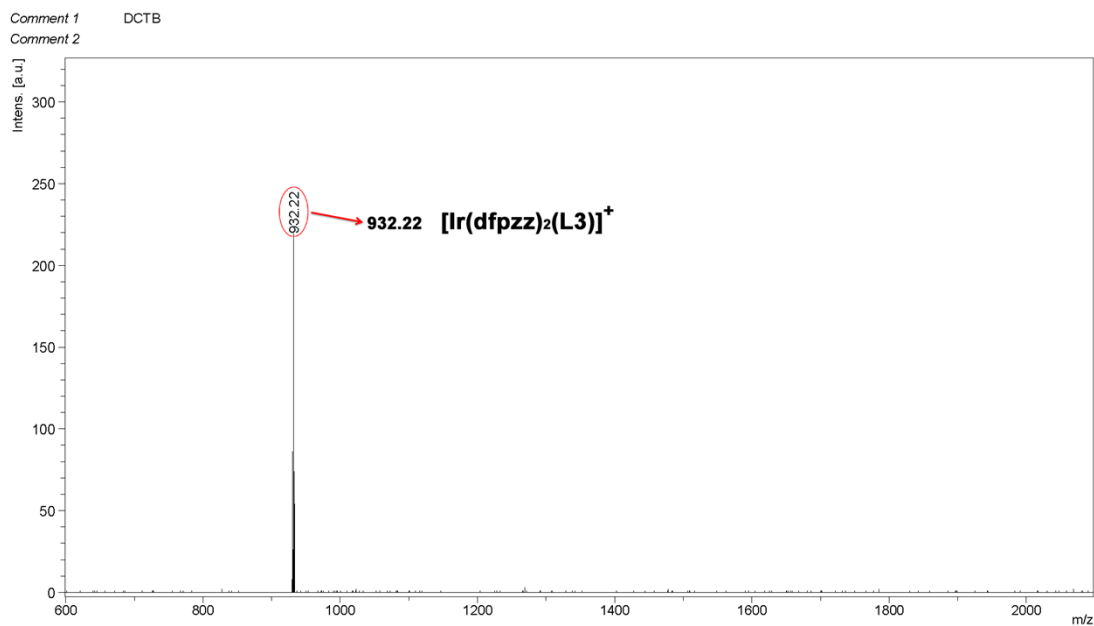


Fig. S3 Copy of the MALDI-TOF MS spectrum for complex **3**.

Table S1. The photoluminescence quantum efficiency (Φ_{PL}) of complexes **1-3** in solutions and in the solid states.

	Photoluminescence quantum efficiency (Φ_{PL})	
	In CH ₃ CN solution	In the solid state
complex 1	9.5%	15.4%
complex 2	nd ^a	23.6%
complex 3	nd ^a	45.3%

^and = not determined because of the weak PL signals.

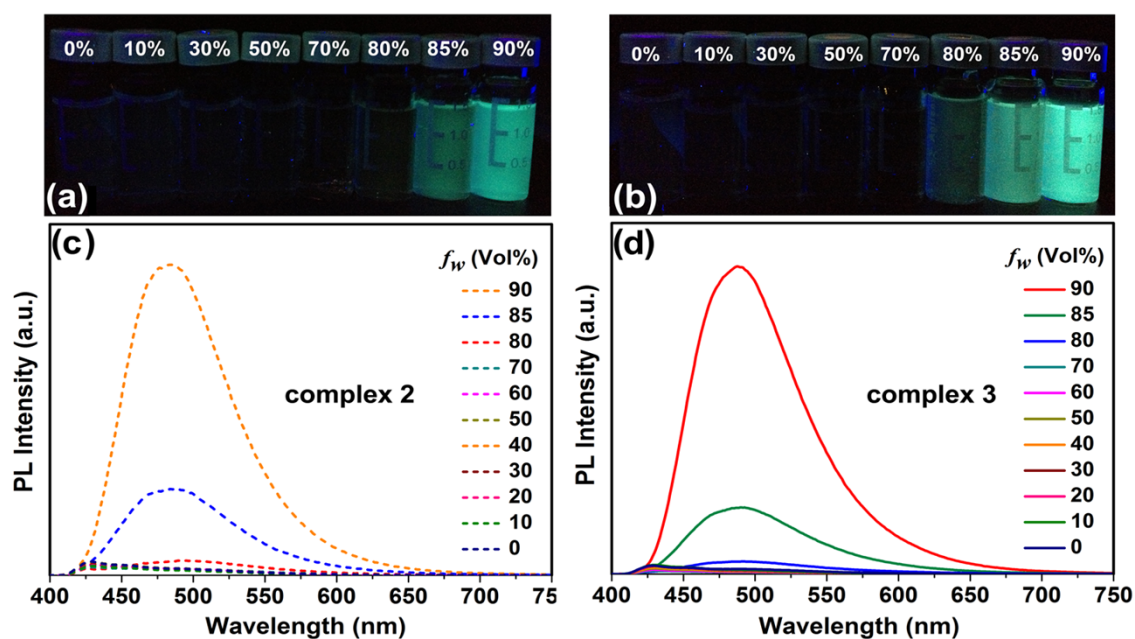


Fig. S4. Luminescent photographs and emission spectra of complexes **2** and **3** in CH₃CN/H₂O mixtures with different water ratio.

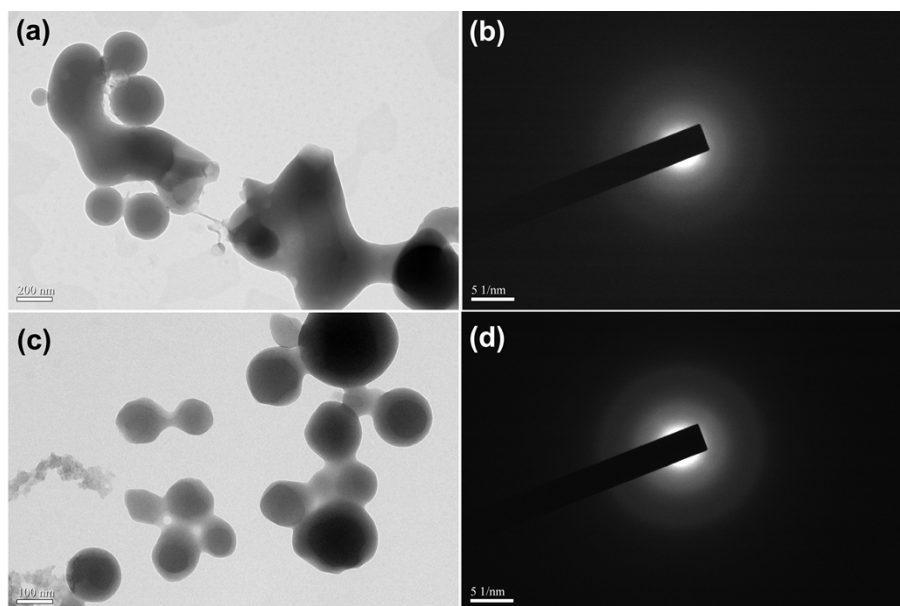


Fig. S5. TEM image of nanoaggregates of complexes **2** (a) and **3** (c) formed in CH₃CN/H₂O mixtures with 90% water fractions. The electron diffraction patterns of the nanoaggregates of complexes **2** (b) and **3** (d).

3. Computational details

Geometry optimizations were performed for the singlet ground state (S_0), the lowest emitting triple excited state (T_1), the lowest 3MC excited state and the transition states for $T_1 \rightarrow ^3MC$ conversions using density functional theory (DFT) at the hybrid functional B3LYP level within the Gaussian 09 software package.¹ The 6-31G* basis sets for C, H, N atoms and the LANL2DZ for Ir atom were selected for the geometry optimization. An effective core potential (ECP) replaces the inner core electrons of iridium leaving the outer core $(5s)^2(5p)^6$ electrons and the $(5d)^6$ valence electrons of Ir(III). The nature of the stationary points was confirmed by computing the Hessian at the same level of theory. Intrinsic reaction coordinate (IRC) calculations were also carried out to confirm the transition states connecting two relevant minima. The minimum energy crossing point (MECP) between the S_0 and the 3MC potential energy surface was optimized using Harvey's algorithm, as implemented in the ORCA software.² For MECP optimizations, the B3LYP functional was employed in combination with the def2-svp basis set and the def2-SD(60,MWB) of Stuttgart-

Dresden scalar relativistic pseudopotential for (C, N, H) and Ir, respectively. To get relative energies for S_0 , T_1 , 3MC , T_s ($T_1 \rightarrow {}^3MC$) and MECP, single-point calculations with the 6-31G* basis set for C, H, N and LANL2DZ for Ir atom were performed.

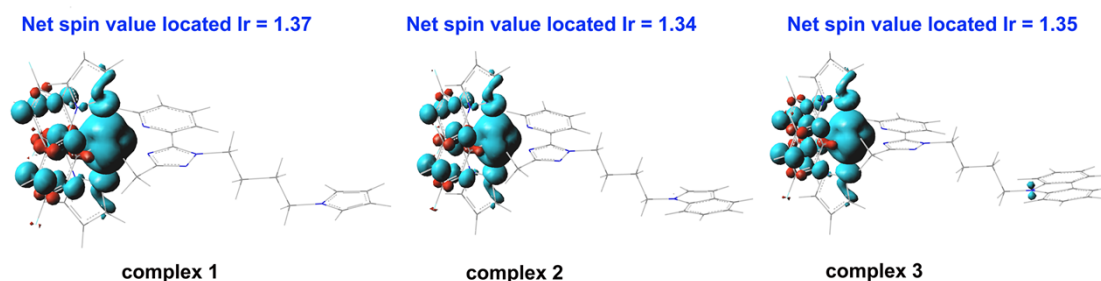
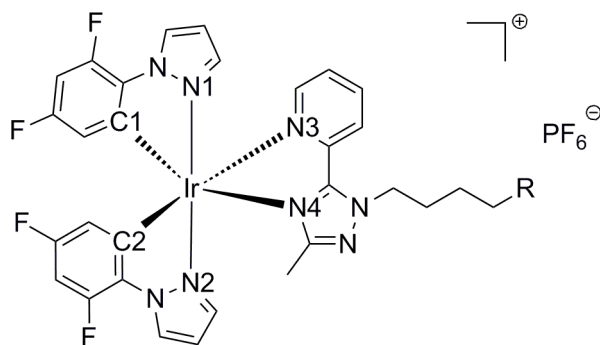


Fig. S6. Spin-density distributions ($0.003 \text{ e}\cdot\text{bohr}^{-3}$) calculated for the 3MC states of complexes **1-3**.

Table S2. Selected bond lengths (in angstroms) calculated for complexes **1-3** in different states.



complex 1					
	S_0	T_1	T_1 - 3MC	3MC	${}^3MC/S_0$
Ir-C1	2.02747	2.01682	2.01219	1.99816	1.99272
Ir-C2	2.02721	2.01513	2.00836	2.01202	2.01707
Ir-N1	2.05449	2.04678	2.35401	2.50454	2.78535
Ir-N2	2.05344	2.04825	2.20527	2.51223	2.73894
Ir-N3	2.23694	2.19144	2.25344	2.25924	2.28271
Ir-N4	2.20875	2.17594	2.19598	2.20411	2.19204

complex 2					
	S ₀	T ₁	T ₁ - ³ MC	³ MC	³ MC/S ₀
Ir-C1	2.02765	2.02023	2.01232	1.99946	1.99536
Ir-C2	2.02740	2.01836	2.01140	2.01271	2.01689
Ir-N1	2.05406	2.04662	2.37613	2.50368	2.78757
Ir-N2	2.05431	2.04809	2.21887	2.51709	2.74265
Ir-N3	2.23671	2.19156	2.24647	2.25508	2.27548
Ir-N4	2.20741	2.17701	2.19545	2.20327	2.19779

complex 3					
	S ₀	T ₁	T ₁ - ³ MC	³ MC	³ MC/S ₀
Ir-C1	2.02796	2.02132	2.01271	1.99979	1.99539
Ir-C2	2.02712	2.01904	2.01152	2.01295	2.01776
Ir-N1	2.05545	2.04732	2.37880	2.50382	2.78413
Ir-N2	2.05348	2.04693	2.21903	2.51183	2.74414
Ir-N3	2.23575	2.19170	2.24258	2.25745	2.27692
Ir-N4	2.21030	2.18016	2.19555	2.20376	2.19476

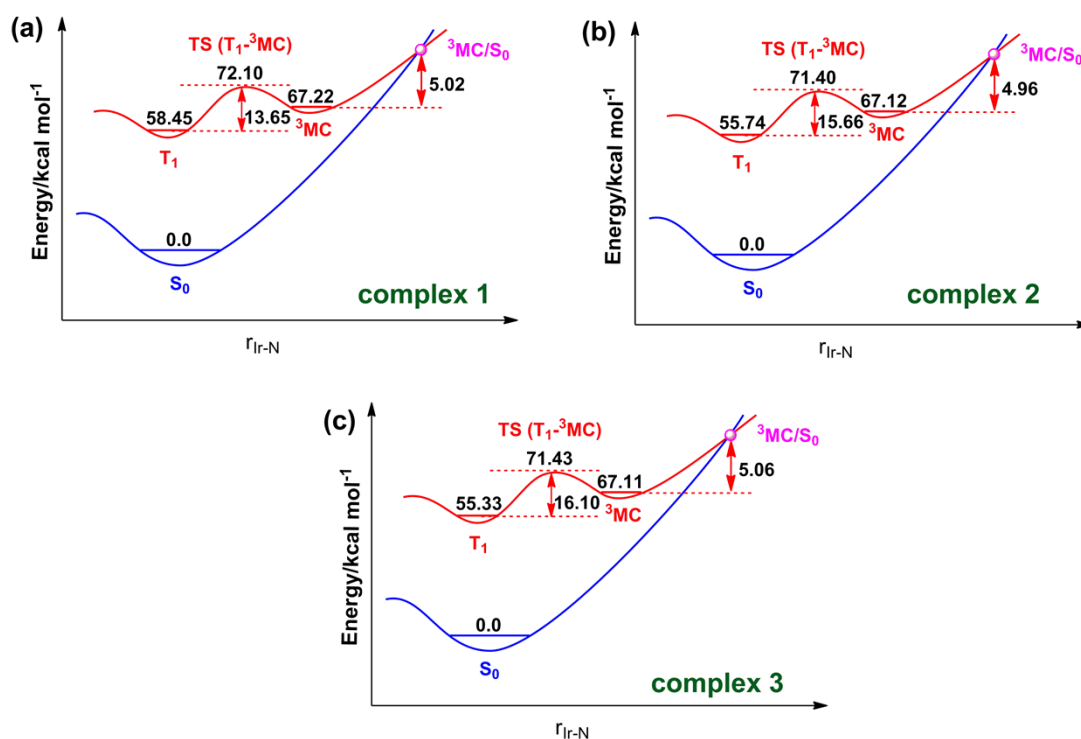


Fig. S7. Schematic potential energy profiles of the deactivation pathway via the ³MC states for complex 1 (a), 2 (b) and 3 (c).

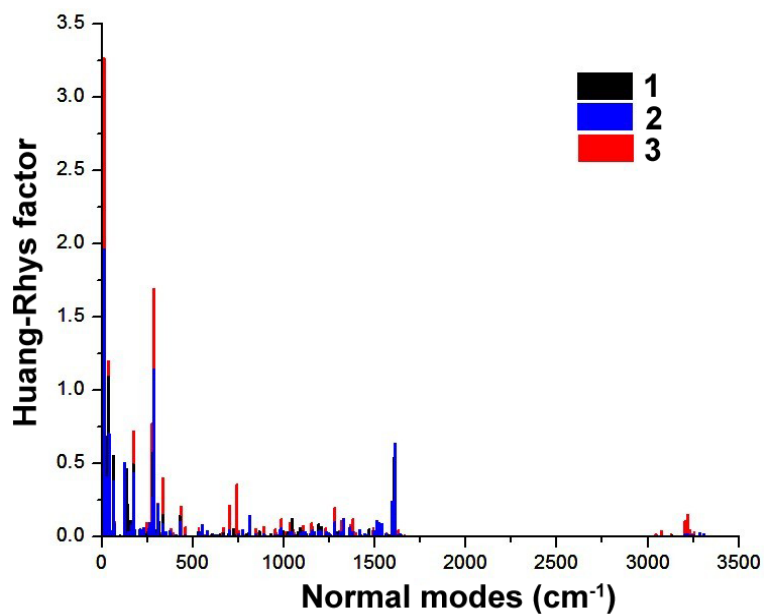


Fig. S8. Calculated Huang-Rhys factors versus the normal mode wave numbers for complexes 1-3.

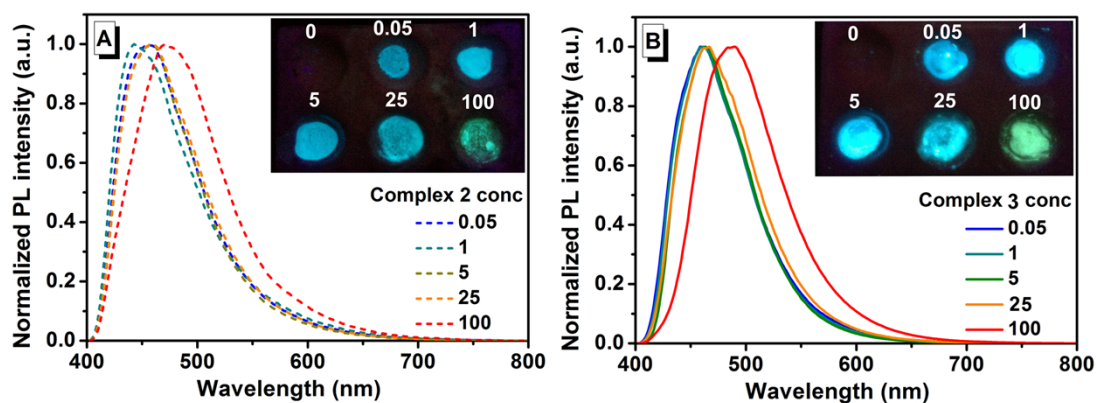


Fig. S9. Emission spectra of complexes 2 (a) and 3 (b) doped PMMA films with different doping ratio (wt%).

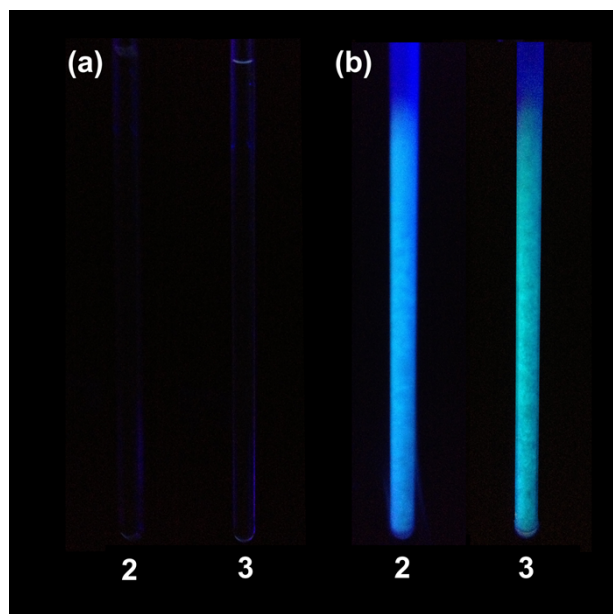


Fig. S10. Luminescent photographs of complexes **2** and **3** in CH₃CN with the concentration of 1×10^{-5} M at room temperature (a) and 77 K (b).

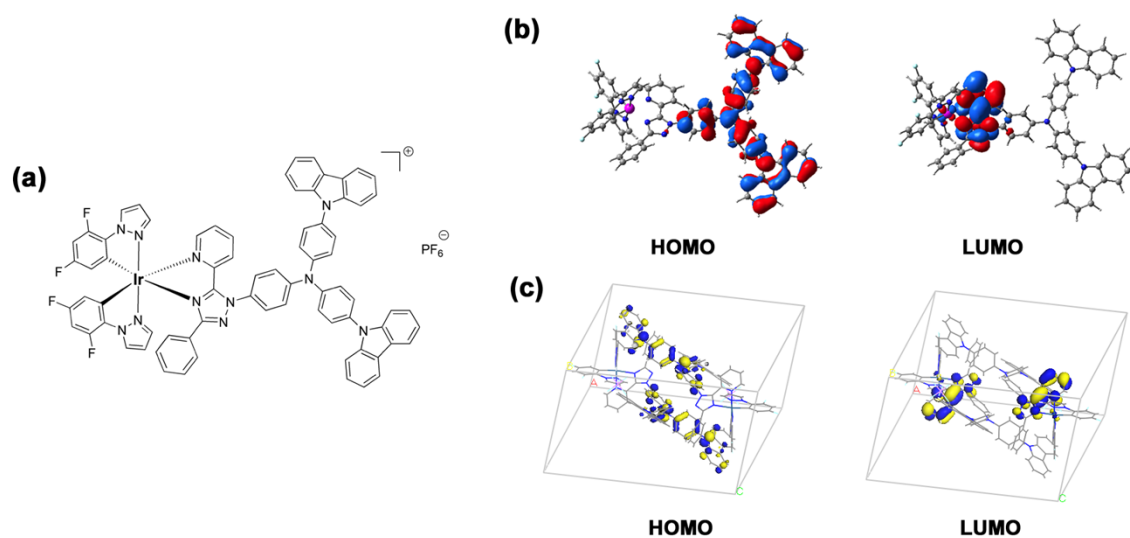


Fig. S11. Chemical structure (a) and HOMO and LUMO orbitals of complex [Ir(dfppz)₂(TRZK)]PF₆ in solution (b) and in crystal state (c), respectively.

References

1. M. J. Frisch, G. W. Trucks, H. B. Schlegel, G. E. Scuseria, M. A. Robb, J. R. Cheeseman, G. Scalmani, V. Barone, B. Mennucci, G. A. Petersson, H. Nakatsuji, M. Caricato, X. Li, H. P. Hratchian, A. F. Izmaylov, J. Bloino, G. Zheng, J. L. Sonnenberg, M. Hada, M. Ehara, K. Toyota, R. Fukuda, J. Hasegawa, M. Ishida, T. Nakajima, Y. Honda, O. Kitao, H. Nakai, T. Vreven, J. A. Montgomery, Jr., J. E. Peralta, F. Ogliaro, M. Bearpark, J. J. Heyd, E. Brothers, K. N. Kudin, V. N. Staroverov, R. Kobayashi, J. Normand, K. Raghavachari, A. Rendell, J. C. Burant, S. S. Iyengar, J. Tomasi, M. Cossi, N. Rega, J. M. Millam, M. Klene, J. E. Knox, J. B. Cross, V. Bakken, C. Adamo, J. Jaramillo, R. Gomperts, R. E. Stratmann, O. Yazyev, A. J. Austin, R. Cammi, C. Pomelli, J. W. Ochterski, R. L. Martin, K. Morokuma, V. G. Zakrzewski, G. A. Voth, P. Salvador, J. J. Dannenberg, S. Dapprich, A. D. Daniels, O. Farkas, J. B. Foresman, J. V. Ortiz, J. Cioslowski and D. J. Fox, Gaussian 09W, Revision A.02; Gaussian, Inc., Wallingford CT, 2009.
2. F. Neese, The ORCA program system, Wiley Interdiscip. Rev.: *Comput. Mol. Sci.*, 2012, **2**, 73.